

# Coulomb bound states of strongly interacting photons

M. F. Maghrebi,<sup>1,\*</sup> M. J. Gullans,<sup>1,\*</sup> P. Bienias,<sup>2</sup> S. Choi,<sup>3</sup> I. Martin,<sup>4</sup>  
O. Firstenberg,<sup>3</sup> M. D. Lukin,<sup>3</sup> H. P. Büchler,<sup>2</sup> and A. V. Gorshkov<sup>1</sup>

<sup>1</sup>*Joint Quantum Institute and Joint Center for Quantum Information and Computer Science,  
NIST/University of Maryland, College Park, Maryland 20742, USA*

<sup>2</sup>*Institute for Theoretical Physics III, University of Stuttgart, Germany*

<sup>3</sup>*Physics Department, Harvard University, Cambridge, Massachusetts 02138, USA*

<sup>4</sup>*Materials Science Division, Argonne National Laboratory, Argonne, Illinois 60439, USA*

We show that two photons coupled to Rydberg states via electromagnetically induced transparency can interact via an effective Coulomb potential. This interaction gives rise to a continuum of two-body bound states. Within the continuum, metastable bound states are distinguished in analogy with quasi-bound states tunneling through a potential barrier. We find multiple branches of metastable bound states whose energy spectrum is governed by the Coulomb potential, thus obtaining a photonic analogue of the hydrogen atom. Under certain conditions, the wavefunction resembles that of a diatomic molecule in which the two polaritons are separated by a finite “bond length.” These states propagate with a negative group velocity in the medium, allowing for a simple preparation and detection scheme, before they slowly decay to pairs of bound Rydberg atoms.

PACS numbers: 42.50.Nn, 32.80.Ee, 34.20.Cf, 42.50.Gy

Photons are fundamental massless particles which are essentially non-interacting for optical frequencies. However, a medium that couples light to its atomic constituents can induce interactions between photons. This interaction may lead to exotic, many-body states of light [1–3], or can be used as a basis for realizing deterministic quantum gates between two photons [4–7]. A promising approach to create strongly interacting photons is to couple the light to atomic Rydberg states [3, 4, 6, 8–36], as realized in recent experiments [37–52].

Rydberg polaritons are superpositions of Rydberg atoms and light, which propagate almost without dissipation under the conditions of electromagnetically induced transparency (EIT) [8, 53–55]. EIT strongly reduces the group velocity and makes Rydberg polaritons dispersive. The large admixture of the Rydberg state can induce strong interactions between polaritons via the inherent Rydberg-Rydberg interactions. Specifically, the blockade effect prevents the formation of two Rydberg polaritons within the so-called “blockade radius” of each other [38, 43, 48, 56–59]. When the probe photons are detuned from the atomic transition, they can form bound states. A shallow bound state of light was observed in recent experiments [45], while stronger interactions result in deep bound states of Rydberg polaritons tied together within the blockaded region [29]. One can imagine these bound states as consisting of a photon trapped by a Rydberg excitation in a deep square well.

In this Letter, we predict and explore a class of photonic states resembling diatomic molecular states in which the two bound photons can be separated by a non-zero “bond length.” This is achieved by considering Rydberg polaritons with the quantized light red-detuned from the excited atomic state. In such a system, we show the existence of metastable bound states exhibit-

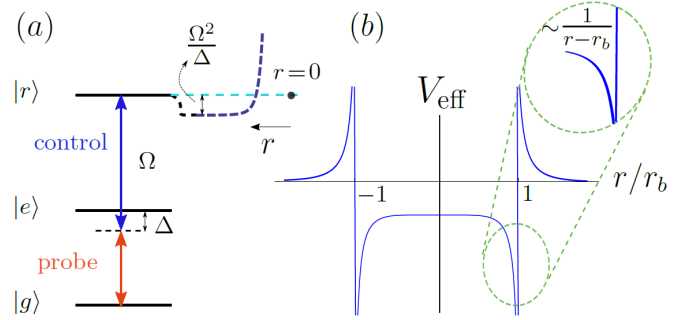


Figure 1: (a) The probe field couples the ground state  $|g\rangle$  to the excited state  $|e\rangle$  and is red-detuned by  $\Delta$ . A control field with Rabi frequency  $\Omega$  couples  $|e\rangle$  to the Rydberg state  $|r\rangle$  and is blue-detuned by  $\Delta$ , thus putting the probe on an EIT transmission resonance. The Rydberg state is thus shifted downward by  $\Omega^2/\Delta$ . The van der Waals interaction with another reference Rydberg excitation at  $r = 0$  can bring  $|r\rangle$  into an absorption resonance with the two-photon transition. (b) The effective potential of two Rydberg polaritons as a function of their separation  $r$ . At large separations, the effective potential is that of the van der Waals interaction; the resonant condition near the blockade radius gives rise to a singularity, while at small separations the interaction levels off as the Rydberg state is highly shifted out of resonance. In the vicinity of the singularity, the potential behaves as that of the Coulomb interaction.

ing the Coulomb spectrum, akin to the hydrogen atom. Such states can potentially be used as building blocks for more complex quantum states of light.

To gain an intuitive understanding, consider the level structure of the Rydberg medium shown in Fig. 1(a). The probe field coupling the ground state  $|g\rangle$  to the intermediate excited state  $|e\rangle$  is red-detuned by  $\Delta > 0$ , and the Rabi frequency of the control field coupling  $|e\rangle$  to the

Rydberg state  $|r\rangle$  is  $\Omega$ . For  $\Omega \ll \Delta$ , the Rydberg state is shifted downward by  $\Omega^2/\Delta$  [see Fig. 1(a)]. The van der Waals interaction  $V(r) = C_6/r^6$  between Rydberg states modifies this picture (we assume  $C_6 > 0$  or more generally  $C_6\Delta > 0$ ). In particular, at small separations  $r$ , the strong interaction shifts two Rydberg states upward and out of resonance, while at large separations, the interaction is negligible and the energy level of each atom asymptotes to  $-\Omega^2/\Delta$  (we set  $\hbar = 1$ ). For intermediate separations on the order of the blockade radius  $r_b$ , defined by  $V(r_b) = 2\Omega^2/\Delta$  [65], the system goes through a resonance (the factor of two arises since both atoms experience the  $\Omega^2/\Delta$  shift). This resonance, associated with a pair (or “molecule”) of Rydberg atoms, endows the effective interaction  $V_{\text{eff}}(r)$  between two Rydberg polaritons with a singularity separating repulsion outside the blockade region from attraction inside; see Fig. 1(b). This effective interaction between two Rydberg polaritons can be roughly thought of as the difference in susceptibility of a single Rydberg polariton with and without a Rydberg excitation at  $r = 0$  [45]. Interestingly, the effective potential near the resonant edge is that of the Coulomb interaction that changes sign across the blockade radius. This potential admits a continuum of states consisting of pairs of bound Rydberg atoms, i.e., Rydberg molecules. Within the continuum, we identify multiple branches of metastable states whose lifetime diverges with the strength of the interaction. When the effective energy of the two-polariton state lies below both  $V_{\text{eff}}(\infty)$  and  $V_{\text{eff}}(0)$ , the bound state experiences a repulsive core and the wavefunction becomes double peaked near  $\pm r_b$ , resembling a diatomic molecular state. We further show that the group velocity of these states is negative, consistent with the fact that they have a finite lifetime.

*Model.*—To describe a propagating polariton in a Rydberg medium, we define  $\mathcal{E}^\dagger(z)$  and  $S^\dagger(z)$  as creation operators for a photon and a Rydberg excitation, respectively, at position  $z$ . We define  $g$  to be the collectively enhanced atom-photon coupling [53] and assume that the decay rates  $\gamma$  of the excited state (satisfying  $\gamma \ll \Delta$ ) and  $\gamma'$  of the Rydberg state can be neglected. In the regime of slow light ( $g \gg \Omega$ ) and with large single-photon detuning ( $\Delta \gg \Omega$ ), one can adiabatically eliminate the excited state  $|e\rangle$  [29, 45]. The two-state Hamiltonian of the Rydberg medium is then

$$H = \int dz \begin{pmatrix} \mathcal{E} \\ S \end{pmatrix}^\dagger \begin{pmatrix} -ic\partial_z + g^2/\Delta & \Omega g/\Delta \\ \Omega g/\Delta & \Omega^2/\Delta \end{pmatrix} \begin{pmatrix} \mathcal{E} \\ S \end{pmatrix} + \frac{1}{2} \int dz dz' V(z-z') S^\dagger(z) S^\dagger(z') S(z') S(z). \quad (1)$$

In the absence of interactions,  $H$  diagonalizes into dark- and bright-state polaritons, where, at low energies, the former ( $\propto gS^\dagger - \Omega\mathcal{E}^\dagger$  when  $\partial_z = 0$ ) is mostly composed of  $|r\rangle$  and travels at a reduced group velocity [53]. In the presence of interactions, the Hamiltonian

in Eq. (1) can be projected onto the sector containing two-particles (at positions  $z$  and  $z'$ ) described by the quantum state  $|\Phi\rangle$  with amplitudes  $EE(z, z')$ ,  $ES(z, z')$ ,  $SE(z, z')$ , and  $SS(z, z')$ , defined in terms of the vacuum  $|0\rangle$  as  $SE(z, z') = \langle 0|S(z)\mathcal{E}(z')|\Phi\rangle$  and similarly for the other amplitudes. The problem is simplified by noting that, for two particles, the total energy  $\omega$  and the center of mass momentum  $K$  are good quantum numbers.

In the limit  $g \rightarrow 0$ , the  $SS$  component decouples from the photonic amplitudes [ $\omega SS(z, z') = (-2\Omega^2/\Delta + V(z-z'))SS(z-z')$ ] giving rise to a continuum of (delta-function) states of Rydberg molecules. (We are making the frozen gas approximation, where we neglect the atomic motion as it is much slower than the polariton dynamics.) Upon increasing  $g$  the continuum of states is still present while the wavefunction remains localized to the blockade radius. To see this, note that the Heisenberg equations of motion for the above amplitudes immediately lead [29, 60] to the Schrödinger-like equation

$$\left[ -\frac{1}{m} \partial_r^2 + \frac{C_6}{r^6 - [r_b(\omega)]^6 + i0^+} \right] \psi(r) = E\psi(r), \quad (2)$$

where  $r$  is the relative coordinate of the two particles, and  $\psi$  is the symmetrized light-Rydberg wavefunction  $\psi(r) \equiv [ES(r) + SE(r)]/2$ . Notice that the van der Waals potential is replaced by an effective potential  $V_{\text{eff}}(r) = C_6/(r^6 - [r_b(\omega)]^6 + i0^+)$  modified within the blockaded region as in Fig. 1(b). For a nonzero  $\omega$ , the blockade radius  $r_b(\omega)$  depends on frequency via the resonant condition  $C_6/[r_b(\omega)]^6 = 2\Omega^2/\Delta + \omega$  (the dependence of  $r_b$  on  $\omega$  will often be implicit below).  $i0^+$  in  $V_{\text{eff}}$  is obtained in the limit of vanishingly small  $\gamma$  and  $\gamma'$ , which is further required by causality. In the limit of small energy and momentum,  $m$  is the mass of a single dark-state polariton due to the curvature of linear susceptibility and is given by  $m = g^4/2c^2\Omega^2\Delta$  [61, 62], while the energy is given by  $E = \omega - v_g K$  with  $v_g = (\Omega^2/g^2)c$  being the EIT group velocity. More generally, the parameters in Eq. (2) can be simply derived from single polariton physics: For two Rydberg dark-state polaritons with momenta  $k_1$  and  $k_2$  and dispersion  $\omega_{1,2} = \omega(k_{1,2})$ , the constraints  $\omega_1 + \omega_2 = \omega$  and  $k_1 + k_2 = K$  yield an expression for the relative momentum  $p = \sqrt{mE}$  consistent with the full, yet complicated, expressions for  $m$  and  $E$  [29, 60]. It is worth pointing out that scattering theory techniques can be used to derive Eq. (2) without adiabatically eliminating the excited state [29], and to show its validity for a wide range of parameters [66]

*Coulomb states.*—The effective potential  $V_{\text{eff}}$  diverges as  $1/(r \pm r_b)$  near the blockade radius, like a Coulomb potential. Across the singularity, the wavefunction  $\psi$  should be continuous, while its derivative does not have to be. The full wavefunction  $\Psi_{\omega, K}(r) = (EE, ES, SE, SS)$  has

various components which are related to  $\psi$  as [29, 45]

$$\begin{aligned} EE(r) &= -\frac{2g\Omega/\Delta}{2g^2/\Delta + \omega - cK} \psi(r), \\ ES(r) &= \left(1 - \frac{ic}{(g^2 + \Omega^2)/\Delta + \omega - cK/2} \partial_r\right) \psi(r), \\ SS(r) &= \frac{2g\Omega}{\Delta C_6} \mathcal{P} \left[ \frac{\psi(r)}{r^{-6} - r_b^{-6}} \right] + \alpha \delta(r \pm r_b), \end{aligned} \quad (3)$$

where, for states with  $\psi(r_b) \neq 0$ , the principal value symbol  $\mathcal{P}$  removes the  $1/[r \pm r_b(\omega)]$  singularity in  $SS$  near the blockade radius. The coefficient  $\alpha$  of the delta-function is determined by the discontinuity in the derivative of  $\psi$  at the blockade radius [60].

We now notice that Eqs. (2,3) admit a special set of solutions, which are a superposition of a normalizable wavefunction vanishing for  $|r| \geq r_b$  [ $\psi(r_b) = 0$ ] and a delta function singularity in the  $SS$  component, but without the  $1/[r \pm r_b(\omega)]$  singularity. Such states can be interpreted in analogy to a *leaky box* where a quasi-bound particle tunnels through a potential barrier: for the leaky box, a true eigenstate is a superposition of the metastable bound state and a plane wave, which is a *momentum* eigenstate selected from a continuum. Similarly, for the above special eigenstates [with  $\psi(r \geq r_b) = 0$ ], the role of the continuum of eigenstates is played by the delta functions in  $SS$ , which are *position* eigenstates. When the delta function is removed, the other components of the wavefunction form a metastable bound state. Furthermore, in the limit of an infinitely strong interaction, i.e.  $g \rightarrow \infty$ , our special eigenstates lose their delta function component [60]. This is again analogous to the leaky box, where, in the limit of an infinitely tall barrier (i.e. the no-leak limit), one obtains exact eigenstates confined to the box and decoupled from the plane-wave component sitting outside the box. Henceforth, we call the metastable bound states above (without the delta function) Coulomb states, and study their spectrum and other properties in detail.

Figure 2(a) shows the energy spectrum of the exact eigenstates (i.e. with the delta function) underlying the Coulomb states. The exact solutions are depicted as solid lines, while the dashed lines show the energy spectrum derived from the WKB quantization condition [applied to the case  $\psi(\pm r_b) = 0$ ]

$$\int_{r_0}^{r_b} p(r) dr = n\pi, \quad n = 1, 2, \dots \quad (4)$$

with  $p(r) = \sqrt{m(E - V_{\text{eff}}(r))}$  defined by Eq. (2), and  $r_0 < r_b$  is the classical turning point near the origin [67]. Figure 2(a) demonstrates that the WKB quantization agrees with the full solution for values of  $K$  near  $2g^2/c\Delta$ .

When  $K$  is close to  $2g^2/c\Delta$ , we can analytically com-

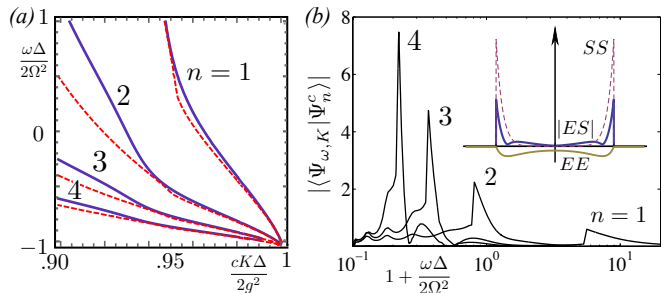


Figure 2: (a) Dispersion curves for the exact eigenstates underlying the metastable Coulomb bound states (only the first four branches  $n = 1-4$  are shown) with  $g^2 r_b / c\Delta = 40$  and  $\Omega/g = 0.05$ . The solid lines give the exact solution, while the dashed lines represent the WKB results. For  $K \rightarrow 2g^2/c\Delta$ , the WKB results are almost exact. The dispersion curves converge to one point with a negative slope, or group velocity. (b) Decomposition of the metastable Coulomb bound states ( $\Psi_n^c$ , defined as  $\Psi_{\omega_n, K_n}$  with the delta-function contribution removed) into the continuum of exact eigenstates. Here we took  $g^2 r_b / c\Delta = 40$  and  $\Omega/g = 0.01$  with a fixed center of mass momentum  $cK\Delta/2g^2 = 0.95$ . The width of these distributions is much less than the energy spacing, a strong indication of metastability. The inset shows the wavefunction components for the  $n = 1$  Coulomb state with the parameters in (a) and  $cK\Delta/2g^2 = 0.98$ . (The  $EE$  component is exaggerated by a factor of 1.5 for better visibility.)

pute the integral in Eq. (4) to find

$$\frac{1 + \omega\Delta/2\Omega^2}{1 - cK\Delta/2g^2} = \mathcal{A} \frac{[g^2 r_b(\omega)/c\Delta]^2}{n^2}, \quad (5)$$

where  $\mathcal{A} = [\Gamma(2/3)/\Gamma(1/6)\sqrt{\pi}]^2 \approx 0.014$ . If  $r_b$  were independent of  $\omega$ , Eq. (5) would imply that  $\omega$  is quantized as  $1/n^2$  (plus a constant), reminiscent of the energy spectrum of the Coulomb potential. However, due to the  $\omega$  dependence of  $r_b$ , the quantization changes to  $\omega_n \sim 1/n^{3/2}$  [68]. The fact that the blockade radius, and, thus, the interaction strength, is sensitive to frequency is a typical feature of nonlinear optical systems [13]. We also stress that  $4g^2 r_b / c\Delta$  is identical to the figure of merit in the far-detuned regime  $OD_b \gamma / \Delta$ , where  $OD_b$  is the optical depth per blockade radius. The figure of merit quantifies the strength of the interaction as two polaritons imprint a phase  $\sim OD_b \gamma / \Delta$  on each other [45].

With the dispersion in hand, we now explore the stability of the Coulomb states. The solutions given by Eq. (3) are a complete set of eigenstates for the two-particle Hilbert space. To normalize these states, we take  $K$  to be fixed and use the energy normalization  $\langle \Psi_{\omega', K} | \Psi_{\omega, K} \rangle = \delta(\omega - \omega')$ . We can then verify the metastability of the Coulomb states ( $\psi[r_b(\omega)] = 0$ ) with the delta-function removed by looking at their decomposition into the normalized eigenstates. Figure 2(b) shows this decomposition for several  $n$ , where we see that the

Coulomb states are sharply peaked at the expected frequencies. The width of these distributions can be much narrower than the spacing between states, a strong signature of spectral distinguishability [63]. Furthermore, the Coulomb states converge to the exact eigenstates for a very strong interaction strength, which is analogous to the leaky box in the limit of an infinitely deep potential [60].

A unique feature of the dispersion curves in Fig. 2(a) is that their slope, and thus the group velocity, is negative. While true eigenstates cannot have a negative group velocity in the absence of left-moving modes (Supplemental Material [60]), Coulomb states are not exact eigenstates and eventually decay into Rydberg molecules. Equation (5) gives the group velocity as  $v = -\mathcal{A}(g^2 r_b / c\Delta)^2 v_g / n^2$ , where  $v_g$  is the EIT group velocity. Therefore, the velocity is also quantized as  $1/n^2$  for different branches of bound states (and fixed values of  $\omega$ ). This quantization and the negative sign make the group velocity an ideal signature for detecting different Coulomb states. We also remark that a small  $\gamma$  ( $\ll \Delta$ ) modifies the energy only slightly, proportional to  $\gamma/\Delta$ , which thus becomes negligible for large detuning.

We now show how to prepare these states and measure their dispersion. We assume that we have access to an additional hyperfine ground state  $|q\rangle$ , which, as shown in Fig. 3(a), is connected to both  $|g\rangle$  and the Rydberg state  $|r\rangle$  through two-photon transitions via an excited state  $|e'\rangle$ . With these additional states, we can effectively turn on and off the polariton interactions by applying a fast  $\pi$ -pulse on the two-photon transition between  $|q\rangle$  and  $|r\rangle$ .

The preparation procedure is as follows. First, we store two identical photons (equivalently a weak coherent state followed by postselection) in the atomic state  $|q\rangle$  using standard protocols [53, 64]. To have a significant overlap with the Coulomb states once we map to  $|r\rangle$ , the state has to have the correct center of mass momentum  $K$ . To achieve this, we introduce a linear energy gradient  $E'$  along the atomic cloud for a time  $\tau$ , which could be achieved with a magnetic field gradient, another optical beam, or microwave field. This will impart a phase  $e^{-iE'\tau R}$  on the stored two-photon state. By choosing the appropriate  $\tau$  and then mapping  $|q\rangle$  to  $|r\rangle$ , we can selectively excite different Coulomb states provided they have a large enough spatial overlap with the initial product state input. As the bound states travel with negative group velocity, the Coulomb state component will separate from the rest of the wavefunction. To detect the state, one can then map the Rydberg state back to  $|q\rangle$  and either measure the population of the state  $|q\rangle$  directly or retrieve the state into light. In Fig. 3(b-d), for realistic parameters (including  $\gamma$  and  $\gamma'$ ) [41], we verify this approach by preparing a variational state that has a large overlap with the  $SS$  component of the Coulomb

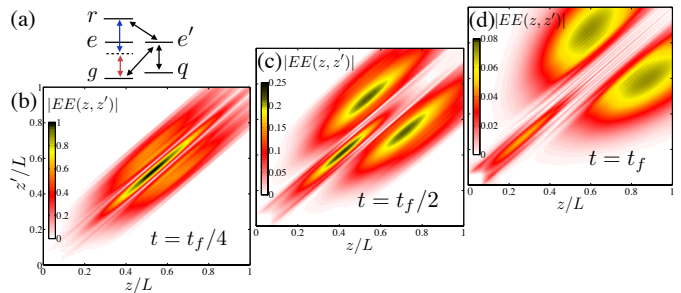


Figure 3: (a) Level structure used to prepare initial  $SS$  distribution. (b-d) Time evolution of a wavepacket with all components initially zero except  $SS$ , which is chosen to be a Gaussian wavepacket of variational  $n = 1$  Coulomb state solutions (with the delta function removed) centered at  $\omega = 0$  and having width  $\Omega^2/2\Delta$  [60]. Specifically,  $|EE\rangle$ , initially zero, is shown after the initial transient evolution subsides at (b)  $t = t_f/4$ , and at (c)  $t = t_f/2$  and (d)  $t = t_f$ , where  $t_f = 10 \Delta/\Omega^2$ . The wavepacket within the blockade radius has the expected shape of the Coulomb state, propagates backward, and decays, while the wavepacket outside the blockade radius propagates forward with  $v_g$  and disperses. We took a medium of length  $L = 16 r_b$ ,  $g^2 r_b / c\Delta = 5$ ,  $g/2\pi = 17$  GHz,  $\Omega/2\pi = 1.5$  MHz,  $r_b = 25 \mu\text{m}$ ,  $\Delta/2\pi = 30$  MHz,  $\gamma/2\pi = 3$  MHz, and  $\gamma'/2\pi = 100$  kHz [45, 60].

state [shown in Fig. 3(b)] with other components equal to zero and solve numerically for the time evolution [60]. In this case, the effective energy  $E$  of the bound state lies above  $V_{\text{eff}}(0)$  and the wavefunction is peaked at  $r = 0$ . We have also verified that, when  $E < V_{\text{eff}}(0)$ , the backward propagating state becomes double peaked and that, for smaller decay rates and larger  $g^2 r_b / c\Delta$ , the negative group velocity observed in the numerics agrees with the WKB prediction from Eq. (4) for the  $n = 1, 2$  and 3 Coulomb states within a few percent in each case [60].

Before concluding, we point out several conditions necessary for the experimental observation of Coulomb states. First, the delta functions appearing in the underlying exact eigenstates should be consistent with the treatment of atoms as a continuous medium. This requires  $\rho(\pi w^2)w_\delta \gg 1$ , where  $\rho$  is the atomic density,  $w$  is the beam waist, and  $w_\delta \sim |dr_b(\omega)/d\omega|/\tau$  is the effective width of the delta function due to the uncertainty in  $\omega$  coming from the finite duration of an experiment  $\tau$ , which is in turn limited by the lifetime of the Coulomb states [ $\sim \Delta/2\Omega^2$  from Fig. 2b]. Recent experiments achieved a density of  $\rho = 2 \times 10^{12} \text{ cm}^{-3}$  with a beam waist of  $w = 4.5 \mu\text{m}$ , corresponding to  $g/2\pi \approx 4$  GHz [45]. We will use below the parameters of Fig. 3, where  $g/2\pi = 17$  GHz, so we will take  $w = 4.5 \mu\text{m}$  and  $\rho = 3.6 \times 10^{13} \text{ cm}^{-3}$ . Taking  $\tau = t_f$ , we then find  $w_\delta \approx 0.2 \mu\text{m}$  and  $\rho(\pi w^2)w_\delta \approx 200$ . Second, two atoms initially  $r_b$  away from each other should not change their distance by more than  $w_\delta$  if they are displaced transversely by  $w$ . This leads to the condition  $w < \sqrt{w_\delta r_b}$ ,

which is nearly satisfied, and can be more strictly satisfied by changing the center frequency of the wavepacket to increase  $r_b(\omega)$ . Finally, the force on a pair of Rydberg atoms  $r_b$  apart and their thermal velocity must both induce motion less than  $w_\delta$  over time  $\tau$ , leading to the conditions  $6C_6\tau^2/(mr_b^7), \tau\sqrt{k_B T}/m < w_\delta$ . Using the mass  $m$  of  $^{87}\text{Rb}$  and temperature  $T = 35 \mu\text{K}$  [41], the first condition is satisfied ( $0.07 \mu\text{m} < 0.2 \mu\text{m}$ ). The second condition can be satisfied by using a sufficiently high control field intensity.

*Outlook.*—While our proposal opens the avenue for the creation of Coulomb-like two-photon states, we expect that a wide class of both useful and exotic two-photon and multi-photon states can be created via refined engineering of photon-photon interactions, e.g. by using microwave fields [43]. The detailed understanding of the two-photon Rydberg-EIT physics provided by this work also opens up an avenue towards understanding the full—and much richer—many-body problem involving an arbitrary number of photons in any dimension.

We thank D. Chang, R. Qi, and Y. Wang for discussions. This work was supported by ARL, NSF PFC at the JQI, the NRC, NSF PIF, CUA, AFOSR, ARO, AFOSR MURI, Center for Integrated Quantum Science and Technology (IQST), the Deutsche Forschungsgemeinschaft (DFG) within SFB TRR 21, the EU Marie Curie ITN COHERENCE, CUA, DARPA QUINNESS, Packard Foundation, and the National Science Foundation. The work of IM was supported by the U.S. Department of Energy, Office of Science, Materials Sciences and Engineering Division.

---

\* These two authors contributed equally.

- [1] I. Carusotto and C. Ciuti, *Rev. Mod. Phys.* **85**, 299 (2013).
- [2] D. E. Chang, V. Gritsev, G. Morigi, V. Vuletić, M. D. Lukin, and E. A. Demler, *Nature Phys.* **4**, 884 (2008).
- [3] J. Otterbach, M. Moos, D. Muth, and M. Fleischhauer, *Phys. Rev. Lett.* **111**, 113001 (2013).
- [4] I. Friedler, D. Petrosyan, M. Fleischhauer, and G. Kurizki, *Phys. Rev. A* **72**, 043803 (2005).
- [5] E. Shahmoon, G. Kurizki, M. Fleischhauer, and D. Petrosyan, *Phys. Rev. A* **83**, 033806 (2011).
- [6] A. V. Gorshkov, J. Otterbach, M. Fleischhauer, T. Pohl, and M. D. Lukin, *Phys. Rev. Lett.* **107**, 133602 (2011).
- [7] D. Paredes-Barato and C. S. Adams, *Phys. Rev. Lett.* **112**, 040501 (2014).
- [8] M. D. Lukin, M. Fleischhauer, R. Cote, L. M. Duan, D. Jaksch, J. I. Cirac, and P. Zoller, *Phys. Rev. Lett.* **87**, 037901 (2001).
- [9] A. E. B. Nielsen and K. Mølmer, *Phys. Rev. A* **81**, 043822 (2010).
- [10] B. Olmos and I. Lesanovsky, *Phys. Rev. A* **82**, 063404 (2010).
- [11] T. Pohl, E. Demler, and M. D. Lukin, *Phys. Rev. Lett.* **104**, 043002 (2010).
- [12] D. Petrosyan, J. Otterbach, and M. Fleischhauer, *Phys. Rev. Lett.* **107**, 213601 (2011).
- [13] S. Sevinçli, N. Henkel, C. Ates, and T. Pohl, *Phys. Rev. Lett.* **107**, 153001 (2011).
- [14] J. Honer, R. Löw, H. Weimer, T. Pfau, and H. P. Büchler, *Phys. Rev. Lett.* **107**, 093601 (2011).
- [15] M. Saffman and T. G. Walker, *Phys. Rev. A* **66**, 065403 (2002).
- [16] L. H. Pedersen and K. Molmer, *Phys. Rev. A* **79**, 012320 (2009).
- [17] J. D. Pritchard, C. S. Adams, and K. Mølmer, *Phys. Rev. Lett.* **108**, 043601 (2012).
- [18] C. Guerlin, E. Brion, T. Esslinger, and K. Mølmer, *Phys. Rev. A* **82**, 053832 (2010).
- [19] J. Stanojevic, V. Parigi, E. Bimbard, A. Ourjoumtsev, P. Pillet, and P. Grangier, *Phys. Rev. A* **86**, 021403 (2012).
- [20] F. Bariani, Y. O. Dudin, T. A. B. Kennedy, and A. Kuzmich, *Phys. Rev. Lett.* **108**, 030501 (2012).
- [21] F. Bariani, P. M. Goldbart, and T. A. B. Kennedy, *Phys. Rev. A* **86**, 041802 (2012).
- [22] J. Stanojevic, V. Parigi, E. Bimbard, A. Ourjoumtsev, and P. Grangier, *Phys. Rev. A* **88**, 053845 (2013).
- [23] M. M. Müller, A. Kölle, R. Löw, T. Pfau, T. Calarco, and S. Montangero, *Phys. Rev. A* **87**, 053412 (2013).
- [24] J.-F. Huang, J.-Q. Liao, and C. P. Sun, *Phys. Rev. A* **87**, 023822 (2013).
- [25] M. Gärttner and J. Evers, *Phys. Rev. A* **88**, 033417 (2013).
- [26] G. W. Lin, J. Yang, X. M. Lin, Y. P. Niu, and S. Q. Gong, arXiv:1308.2782 (2013).
- [27] A. V. Gorshkov, R. Nath, and T. Pohl, *Phys. Rev. Lett.* **110**, 153601 (2013).
- [28] B. He, A. Sharypov, J. Sheng, C. Simon, and M. Xiao, *Phys. Rev. Lett.* **112**, 133606 (2014).
- [29] P. Bienias, S. Choi, O. Firstenberg, M. F. Maghrebi, M. Gullans, M. D. Lukin, A. V. Gorshkov, and H. P. Büchler, *Phys. Rev. A* **90**, 053804 (2014).
- [30] M. Gärttner, S. Whitlock, D. W. Schönleber, and J. Evers, *Phys. Rev. A* **89**, 063407 (2014).
- [31] Y.-M. Liu, D. Yan, X.-D. Tian, C.-L. Cui, and J.-H. Wu, *Phys. Rev. A* **89**, 033839 (2014).
- [32] A. Grankin, E. Brion, E. Bimbard, R. Boddeda, I. Usmani, A. Ourjoumtsev, and P. Grangier, *New J. Phys.* **16**, 043020 (2014).
- [33] W. Li, D. Viscor, S. Hofferberth, and I. Lesanovsky, *Phys. Rev. Lett.* **112**, 243601 (2014).
- [34] H. Wu, M.-M. Bian, L.-T. Shen, R.-X. Chen, Z.-B. Yang, and S.-B. Zheng, *Phys. Rev. A* **90**, 045801 (2014).
- [35] G. W. Lin, J. Gong, J. Yang, Y. H. Qi, X. M. Lin, Y. P. Niu, and S. Q. Gong, *Phys. Rev. A* **89**, 043815 (2014).
- [36] I. I. Beterov, T. Andrijauskas, D. B. Tretyakov, V. M. Entin, E. A. Yakshina, I. I. Ryabtsev, and S. Bergamini, *Phys. Rev. A* **90**, 043413 (2014).
- [37] J. D. Pritchard, D. Maxwell, A. Gauguier, K. J. Weatherill, M. P. A. Jones, and C. S. Adams, *Phys. Rev. Lett.* **105**, 193603 (2010).
- [38] Y. O. Dudin and A. Kuzmich, *Science* **336**, 887 (2012).
- [39] Y. O. Dudin, F. Bariani, and A. Kuzmich, *Phys. Rev. Lett.* **109**, 133602 (2012).
- [40] Y. O. Dudin, L. Li, F. Bariani, and A. Kuzmich, *Nature Phys.* **8**, 790 (2012).
- [41] T. Peyronel, O. Firstenberg, Q.-Y. Liang, S. Hofferberth, A. V. Gorshkov, T. Pohl, M. D. Lukin, and V. Vuletic, *Nature (London)* **488**, 57 (2012).
- [42] V. Parigi, E. Bimbard, J. Stanojevic, A. J. Hilliard,

- F. Nogrette, R. Tualle-Broui, A. Ourjoumtsev, and P. Grangier, *Phys. Rev. Lett.* **109**, 233602 (2012).
- [43] D. Maxwell, D. J. Szwer, D. Paredes-Barato, H. Busche, J. D. Pritchard, A. Gauguet, K. J. Weatherill, M. P. A. Jones, and C. S. Adams, *Phys. Rev. Lett.* **110**, 103001 (2013).
- [44] C. S. Hofmann, G. Günter, H. Schempp, M. Robert-de Saint-Vincent, M. Gärttner, J. Evers, S. Whitlock, and M. Weidemüller, *Phys. Rev. Lett.* **110**, 203601 (2013).
- [45] O. Firstenberg, T. Peyronel, Q.-Y. Liang, A. V. Gorshkov, M. D. Lukin, and V. Vuletic, *Nature (London)* **502**, 71 (2013).
- [46] G. Günter, H. Schempp, M. Robert-de Saint-Vincent, V. Gavryusev, S. Helmrich, C. S. Hofmann, S. Whitlock, and M. Weidemüller, *Science* **342**, 954 (2013).
- [47] H. Gorniaczyk, C. Tresp, J. Schmidt, H. Fedder, and S. Hofferberth, *Phys. Rev. Lett.* **113**, 053601 (2014).
- [48] P. Schausz, M. Cheneau, M. Endres, T. Fukuhara, S. Hild, A. Omran, T. Pohl, C. Gross, S. Kuhr, and I. Bloch, *Nature* **491**, 87 (2012).
- [49] S. Baur, D. Tiarks, G. Rempe, and S. Dürr, *Phys. Rev. Lett.* **112**, 073901 (2014).
- [50] P. Schauf, J. Zeiher, T. Fukuhara, S. Hild, M. Cheneau, T. Macrì, T. Pohl, I. Bloch, and C. Gross, *arXiv:1404.0980* (2014).
- [51] D. Tiarks, S. Baur, K. Schneider, S. Dürr, and G. Rempe, *Phys. Rev. Lett.* **113**, 053602 (2014).
- [52] D. Maxwell, D. J. Szwer, D. Paredes-Barato, H. Busche, J. D. Pritchard, A. Gauguet, M. P. A. Jones, and C. S. Adams, *Phys. Rev. A* **89**, 043827 (2014).
- [53] M. Fleischhauer and M. D. Lukin, *Phys. Rev. Lett.* **84**, 5094 (2000).
- [54] M. Fleischhauer, A. Imamoglu, and J. P. Marangos, *Rev. Mod. Phys.* **77**, 633 (2005).
- [55] M. Saffman, T. G. Walker, and K. Mølmer, *Rev. Mod. Phys.* **82**, 2313 (2010).
- [56] A. Gaetan, Y. Miroshnychenko, T. Wilk, A. Chotia, M. Viteau, D. Comparat, P. Pillet, A. Browaeys, and P. Grangier, *Nature Phys.* **5**, 115 (2013).
- [57] E. Urban, T. A. Johnson, T. Henage, L. Isenhower, D. D. Yavuz, T. G. Walker, and M. Saffman, *Nature Phys.* **5**, 110 (2013).
- [58] H. Schempp, G. Günter, M. Robert-de Saint-Vincent, C. S. Hofmann, D. Breyel, A. Komnik, D. W. Schönleber, M. Gärttner, J. Evers, S. Whitlock, et al., *Phys. Rev. Lett.* **112**, 013002 (2014).
- [59] R. Heidemann, U. Raitzsch, V. Bendkowsky, B. Butscher, R. Löw, L. Santos, and T. Pfau, *Phys. Rev. Lett.* **99**, 163601 (2007).
- [60] See Supplemental Material at <http://link.aps.org/supplemental/???> for details omitted in the main text.
- [61] F. E. Zimmer, A. André, M. D. Lukin, and M. Fleischhauer, *Opt. Comm.* **264**, 441 (2006).
- [62] F. E. Zimmer, J. Otterbach, R. G. Unanyan, B. W. Shore, and M. Fleischhauer, *Phys. Rev. A* **77**, 063823 (2008).
- [63] M. Razavy, *Quantum theory of tunneling* (World Scientific, 2003).
- [64] A. V. Gorshkov, A. André, M. D. Lukin, and A. S. Sørensen, *Phys. Rev. A* **76**, 033804 (2007).
- [65] For notational convenience, this definition differs from that in Refs. [6, 45] by the presence of the factor of 2 on the right-hand side.
- [66] The Schrödinger equation is an excellent approximation as long as  $1 - cK\Delta/2g^2 \gtrsim \Omega^3/\Delta^3$  [29], i.e., even for  $K$  close to  $2g^2/c\Delta$ .
- [67] If no turning point exists,  $r_0 = 0$ , and the quantization condition changes as  $n \rightarrow n - 1/4$ .
- [68] A more appropriate way of seeing the energy quantization is to look at the difference between  $\omega$  on different branches cut by a line perpendicular to the dispersion curves when  $\omega$  and  $K$  are normalized in units of  $2\Omega^2/\Delta$  and  $2g^2/c\Delta$ , respectively, and for  $cK\Delta/2g^2 \rightarrow 1$ . One then recovers  $\omega_n \sim 1/n^2$ .



# Supplemental Material for ‘‘Coulomb bound states of strongly interacting photons’’

## I. ADIABATIC ELIMINATION

In this section, we derive the Shrödinger equation (2) of the main text.

Upon adiabatic elimination of the intermediate state  $|e\rangle$ , the two-particle wave function is described by four components  $EE$ ,  $ES$ ,  $SE$ , and  $SS$ , each of which is a function of time and two spatial coordinates. We define  $ES_{\pm} = (ES \pm SE)/2$  as the symmetric and antisymmetric combinations of the photon-Rydberg components. In the frequency domain, the Heisenberg equations can be cast as (see Refs. [S1]-[S4] for more details)

$$\omega EE = -ic\partial_R EE - \frac{2g^2}{\Delta} EE - \frac{2g\Omega}{\Delta} ES_+, \quad (S1)$$

$$\begin{aligned} \omega ES_+ &= -\frac{ic}{2}\partial_R ES_+ - \frac{g^2 + \Omega^2}{\Delta} ES_+ \\ &\quad - ic\partial_r ES_- - \frac{g\Omega}{\Delta} (EE + SS), \end{aligned} \quad (S2)$$

$$\omega ES_- = -\frac{ic}{2}\partial_R ES_- - \frac{g^2 + \Omega^2}{\Delta} ES_- - ic\partial_r ES_+, \quad (S3)$$

$$\omega SS = -\frac{2\Omega^2}{\Delta} SS + V(r)SS - \frac{2g\Omega}{\Delta} ES_+, \quad (S4)$$

where  $\omega$  is the frequency,  $r = z - z'$  denotes the relative coordinate, and  $R = (z + z')/2$  is the center of mass coordinate. For an infinitely long medium, one can work in Fourier space (relative to  $R$ ) with the total momentum  $K$ . Defining  $\psi(r) = ES_+(r)$ , Eqs. (S1,S3,S4) yield, respectively,

$$EE = -\frac{2g\Omega}{\Delta} \frac{1}{\frac{2g^2}{\Delta} + \omega - cK} \psi, \quad (S5)$$

$$ES_- = \frac{-ic}{\frac{g^2 + \Omega^2}{\Delta} + \omega - \frac{Kc}{2}} \partial_r \psi, \quad (S6)$$

$$SS = -\frac{2g\Omega}{\Delta} \mathcal{P} \left[ \frac{\psi}{\frac{2\Omega^2}{\Delta} + \omega - V(r)} \right] + \alpha \delta[r - r_b(\omega)], \quad (S7)$$

with  $\mathcal{P}$  denoting the principal part near the singularity at the blockade radius. The coefficient  $\alpha$  is determined by matching boundary conditions across the singularity. Inserting these expressions into Eq. (S2), we obtain a second-order differential equation for  $\psi$  as

$$-\frac{1}{m} \partial_r^2 \psi + V_{\text{eff}}(r)\psi = E\psi, \quad (S8)$$

which is valid everywhere away from the blockade radius, i.e. for  $|r| > r_b(\omega)$  and  $|r| < r_b(\omega)$ . The effective potential is given by

$$V_{\text{eff}}(r) = \frac{V(r)}{1 - V(r)/(\frac{2\Omega^2}{\Delta} + \omega)}, \quad (S9)$$

which, for  $C_6\Delta > 0$ , reduces to the effective potential in Eq. (2) of the main text. Defining the normalized units  $\bar{\omega} = \omega\Delta/2\Omega^2$  and  $\bar{K} = cK\Delta/2g^2$ , the values of the energy and the mass take the form

$$E = \frac{2\Omega^2}{\Delta} (1 + \bar{\omega})^2 \quad (S10)$$

$$\begin{aligned} &\times \left[ 1 - \bar{K} + \frac{\Omega^2}{g^2} (1 + 2\bar{\omega}) - \frac{\Omega^2/g^2}{1 - \bar{K} + \bar{\omega}\Omega^2/g^2} - \frac{1}{1 + \bar{\omega}} \right], \\ m &= \frac{g^4}{2\Omega^2\Delta c^2} \frac{1}{(1 + \bar{\omega})^2} \left[ 1 - \bar{K} + \frac{\Omega^2}{g^2} (1 + 2\bar{\omega}) \right]. \end{aligned} \quad (S11)$$

These expressions also fully agree with the diagrammatic approach of Ref. [S4] in the above limits.

The boundary conditions at the origin [ $\psi'(0) = 0$ ] and at infinity [ $\psi(r \rightarrow \infty) = 0$ ] are necessary to solve for  $\psi$ . Furthermore, the wavefunction should be continuous across the singularity at  $r = r_b$ . On the other hand, the discontinuity in its first derivative at  $r = r_b$  determines the coefficient  $\alpha$ , via Eqs. (S2,S3,S7), as

$$\alpha = -\frac{\Delta c/g\Omega}{(g^2 + \Omega^2)/\Delta c + \omega/c - K/2} \partial_r \psi \Big|_{r_b^-}^{r_b^+}. \quad (S12)$$

## II. BOUNDARY CONDITION AT THE SINGULARITY

In this section, we show how to explicitly calculate  $\partial_r \psi \Big|_{r_b^-}^{r_b^+}$ , and hence determine  $\alpha$  via Eq. (S12), taking into account the boundary conditions at  $r = 0$  and  $r = \infty$ . This is necessary for constructing the eigenbasis used in Fig. 2(b) of the main text.

Because of the singularity in  $V_{\text{eff}}$ , we find that  $\alpha$  has both real and imaginary parts which can never simultaneously vanish. This implies that all eigenstates have a delta-function contribution. To show this, consider a small neighborhood near the singularity where Eq. (S8) takes the form

$$\frac{1}{U^2} \partial_x^2 \psi = \frac{1}{x-1} \psi, \quad (S13)$$

with  $U \approx \frac{g^2 r_b(\omega)}{\sqrt{6}\Delta c} \sqrt{\frac{1-cK\Delta/2g^2}{1+\omega\Delta/2\Omega^2}}$  and  $x = r/r_b(\omega)$ . This equation is valid for  $|x-1| \ll 1$  and has analytic solutions on both sides of the singularity in terms of first

order Bessel functions

$$\psi_1^-(x) \approx \frac{\sqrt{1-x}}{U} J_1(2U\sqrt{1-x}), \quad (\text{S14})$$

$$\psi_2^-(x) \approx -\frac{\pi\sqrt{1-x}}{U} Y_1(2U\sqrt{1-x}), \quad (\text{S15})$$

$$\psi_1^+(x) \approx \frac{\sqrt{x-1}}{U} I_1(2U\sqrt{x-1}), \quad (\text{S16})$$

$$\psi_2^+(x) \approx \frac{2\sqrt{x-1}}{U} K_1(2U\sqrt{x-1}), \quad (\text{S17})$$

where  $\mp$  refers to  $x \lesseqgtr 1$ , and the  $\approx$  signs are meant to indicate that these equalities hold only for  $|x-1| \ll 1$ . The solutions  $\psi$  for all  $x$  are obtained by using Eq. (S8) to extend the above  $\psi_{1,2}^\pm$  to all  $x$ . One then imposes the boundary conditions that  $\psi$  is symmetric about  $x=0$ , i.e.,  $d\psi/dx(x=0)=0$ , and  $\psi(x) \rightarrow 0$  as  $x \rightarrow \infty$ . The solution for  $x < 1$  can be written as

$$\psi(x) = c_1 \psi_1^-(x) + c_2 \psi_2^-(x), \quad (\text{S18})$$

where  $c_1$  and  $c_2$  are determined by the boundary condition at  $x=0$ . For  $x > 1$ , one can show that the choice of  $\psi_2^+$  in terms of the Bessel function of the second kind  $K_1$  near the singularity guarantees that, away from the singularity where Eqs. (S15)-(S17) are no longer valid,  $\psi_2^+$  decays exponentially for large values of  $x$ , while  $\psi_1^+$  grows exponentially. Imposing the boundary condition that  $\psi$  vanishes at infinity implies  $\psi(x) \propto \psi_2^+(x)$ , while the continuity of  $\psi(x)$  at  $x=1$  gives the result

$$\psi(x) = \begin{cases} c_1 \psi_1^-(x) + c_2 \psi_2^-(x), & x < 1, \\ c_2 \psi_2^+(x), & x > 1. \end{cases} \quad (\text{S19})$$

The contribution of  $\psi_1^\pm$  to  $\partial_x \psi|_{1^\pm}^{1^\pm}$  is  $c_1$ . However, calculating the contribution of  $\psi_2^\pm$  to  $\partial_x \psi|_{1^\pm}^{1^\pm}$  requires more care because, near the singularity,  $\partial_x \psi_2^\pm \sim \log(1-x)$ . To help resolve this, we examine the solutions in the presence of an infinitesimal decay rate  $\gamma'$  from the Rydberg state. In this case, near the singularity, the effective Schrödinger equation takes the form

$$\frac{1}{U^2} \partial_x^2 \psi = \frac{1}{x-1+i\epsilon} \psi, \quad (\text{S20})$$

where  $\epsilon = \gamma' / (\omega + 2\Omega^2/\Delta)$ . Using the relation

$$\lim_{\epsilon \rightarrow 0} \frac{1}{x-1+i\epsilon} = \mathcal{P}\left(\frac{1}{x-1}\right) - i\pi\delta(x-1), \quad (\text{S21})$$

and integrating Eq. (S20) across the singularity suggests a contribution to  $\partial_x \psi|_{1^-}^{1^+}$  equal to  $-i\pi U^2 \psi(1) = -i\pi c_2$ . Combining this result with the  $c_1$  contribution gives

$$\alpha = -\frac{\Delta c/g\Omega r_b}{(g^2 + \Omega^2)/\Delta c + \omega/c - K/2} (c_1 - i\pi c_2). \quad (\text{S22})$$

With this final result, we can construct the complete set of states used in making Fig. 2(b) of the main text. First,

we solve numerically for  $\psi$  inside the blockade radius. We then find  $c_1$  and  $c_2$  by matching these numerical solutions, in a region near the singularity, to the analytic solutions in Eqs. (S14)-(S15). To check the arguments presented above, we have also verified numerically that when the imaginary component to  $\alpha$  is neglected the resulting solutions do not form an orthonormal basis, while, when the imaginary term is included, the solutions are consistent with an orthonormal basis.

Since  $c_{1,2}$  can be assumed to be real numbers, which cannot both vanish, it is clear that all eigenstates have the delta-function contribution. This is consistent with the fact that, for  $g=0$ , the continuum is composed of Rydberg molecule states. For finite  $g$ , these states become dressed with the photons, but do not lose their character as atomic bound states. The eigenstates linked to the Coulomb states have the special property that  $c_2 = U^2 \psi(1) = 0$ .

From this solution, we can also determine the behavior of the eigenstates as the interaction strength  $U \rightarrow \infty$ . At the singularity,  $\psi(1) = c_2/U^2$ , which implies that, as  $U$  increases,  $\psi(1) \rightarrow 0$  and all solutions satisfy the same boundary condition at the singularity. Additionally, in this limit  $\alpha \rightarrow 0$ , which implies that the states confined inside the Rydberg blockade completely decouple from the continuum of Rydberg molecule states (i.e., the delta functions). This is again analogous to the leaky box discussed in the main text, where, as the box becomes infinitely deep, the eigenstates inside the well become decoupled from the continuum of momentum states that live outside the box.

### III. NUMERICAL METHODS

In this section, we describe the numerical methods used to obtain Fig. 3 of the main text.

We include the decay rate  $\gamma$  of the intermediate state by adding an imaginary component to  $\Delta$ . Decay of the Rydberg state requires adding the term  $-i(\gamma'/2) \int dz S^\dagger(z) S(z)$  to the Hamiltonian.

Within the two-excitation subspace,  $H$  can be split into a kinetic term  $T$  that describes the propagation of photons and a part  $W$  that is diagonalizable in real space, that includes the Rydberg-Rydberg interaction, decay, and coupling to the quantum and classical light fields. We can then find the time-evolution of the wavefunction by a Trotter decomposition, whereby we split the propagator into two parts which are separably diagonalizable in momentum ( $T$ ) and real-space ( $W$ )

$$e^{-iH\tau} \approx e^{-iT\tau/2} e^{-iW\tau} e^{-iT\tau/2} + O([W, T] \tau^2). \quad (\text{S23})$$

In our case,  $\mathcal{E}$  has a linear dispersion, which implies that propagation with  $T$  corresponds to a uniform shift in real-space of the  $\mathcal{E}$ -components of the wavefunction, while



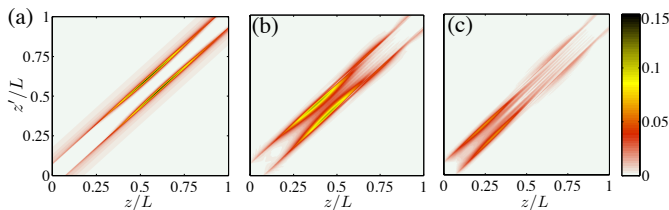


Figure S1: Time evolution of the  $n = 1$  Coulomb state as in Fig. 3 of the main text, except here we take a much larger value of  $g^2 r_b/c\Delta$  and much smaller decay rates to verify that our analytical theory accurately describes the Coulomb states. The initial condition for  $EE$ ,  $ES$ , and  $SE$  is chosen to be zero, while  $SS$  is chosen to be given by Eq. (S24) with  $\sigma = \Omega^2/2\Delta$  and  $n = 1$ . The  $|EE|$  component is shown (a) shortly after  $t = 0$  at  $tv_g/L = 10^{-4}$  and at later times (b)  $tv_g/L = 3 \cdot 10^{-3}$  and (c)  $tv_g/L = 6 \cdot 10^{-3}$ . Here  $L$  is the length of the medium, and we took  $g^2 r_b/c\Delta = 40$ ,  $\Omega/g = 0.05$ ,  $L/r_b = 14$ ,  $\Omega/\Delta = 0.25$ ,  $\gamma/\Delta = 0.05$ , and  $\gamma'/\Delta = 0.01$ . For these parameters, in contrast to those of Fig. 3 in the main text, the  $EE$  component of the Coulomb state is localized near the blockade radius.

$e^{-iW\tau}$  can be found exactly for each point in space. Using these solutions, we can construct the long-time-evolution by stepwise application of Eq. (S23) for small  $\tau$ .

For the experimental parameters in Fig. 3 of the main text, the group velocity  $v_g/c \approx \Omega^2/g^2 \approx 10^{-8}$ , which implies that there is a large separation of time scales between the light propagation and the atomic dynamics. Just increasing the time step cannot overcome this because the error term in the Trotter decomposition becomes very large. This problem can, however, be overcome by bringing the time scales closer together through the scaling transformation  $z \rightarrow \zeta z$ ,  $g \rightarrow g/\sqrt{\zeta}$ , and  $r_b \rightarrow \zeta r_b$ . One can see from Eqs. (S10-S11) that the dynamics are invariant under this transformation provided  $v_g\zeta/c \ll (1 - \bar{K})^2$ . To obtain Fig. 3 of the main text, we use  $\zeta = 1.2 \times 10^7$ , which satisfies this condition.

The observation of Coulomb states requires large interaction strengths (equivalently atomic densities). This in turn requires a fine numerical mesh for the wavefunction, which makes the simulations very time consuming. However, since the Coulomb states are confined to a region on the order of the blockade radius we can force the wavefunction to be zero outside a region on the order of a few blockade radii. This significantly reduces the required memory and simulation time. We have verified that our numerical results are insensitive to this cutoff.

Finally,  $H$  is an effective Hamiltonian obtained after adiabatically eliminating the intermediate state  $|e\rangle$ . We have also verified numerically that our results hold when state  $|e\rangle$  is explicitly included in the simulations.

#### IV. CONDITION FOR REPULSIVE CORE

In this section, we establish the parameter regime when the effective energy  $E < V_{\text{eff}}(0)$ . In this case, the two-photon state feels a repulsive core and becomes peaked near the points  $\pm r_b$ . From Eq. (S10) and Eq. (S11) we can see that, for  $\Omega^2/g^2 \ll 1$ , we can rewrite

$$E - V_{\text{eff}}(0) \approx \frac{2\Omega^2}{\Delta} \frac{(1 + \bar{\omega})^2}{1 - \bar{K}} [(1 - \bar{K})^2 - \Omega^2/g^2],$$

which becomes negative when  $1 - \bar{K} < \Omega/g$ . Note that, in order for the adiabatic elimination to be valid near  $\bar{K} = 1$ , we also require  $1 - \bar{K} \gg \Omega^3/\Delta^3$  [S4]. This sets the constraints  $\Omega/g > 1 - \bar{K} \gg \Omega^3/\Delta^3$ , in order to have a repulsive core, which can be easily satisfied.

In Fig. S1 we show the resulting backward propagating state under the same preparation procedure as described in the main text and Fig. 3, except in this case we took smaller decay rates, a larger value of  $g^2 r_b/c\Delta$  and a much larger control field intensity. In particular, the Coulomb state we prepared had  $1 - \bar{K} \approx 0.02$  and  $\Omega/g = 0.05$ . The double peaked structure is clearly visible, consistent with the presence of the repulsive core for this bound state.

#### V. GROUP VELOCITY OF COULOMB STATES

In this section, we compare the group velocity predicted by the WKB treatment in the main text with numerical simulations for  $n = 1, 2$ , and 3. To construct the Coulomb wavepacket, we first choose a narrow range of frequencies around  $\omega = 0$  and, for every  $\omega$ , we find  $K_n(\omega)$  from Eq. (4) in the main text, which gives us an expression for  $p_n(r, \omega)$ . The initial state has  $EE = ES = SE = 0$  with  $SS$  given by the variational wavefunction

$$SS_n(r, R) = \mathcal{N} \int d\omega e^{iK_n(\omega)R - \omega^2/\sigma^2} \frac{1}{1 - [r_b(\omega)/r]^6} \times \left[ (-1)^n - \cos \int_0^r p_n(r, \omega) \right] \Theta[r - r_b(\omega)], \quad (\text{S24})$$

which vanishes at  $r_b(\omega)$  for every  $\omega$ . Here  $\mathcal{N}$  is a normalization constant,  $\sigma$  is the width of the wavepacket, and  $\Theta$  is the Heaviside step function.

The results are shown in Fig. 3 of the main text and in Figs. S1-S2. Fig. 3 of the main text and Fig. S1 show snapshots of the backward-propagating  $n = 1$  wavefunction. While Fig. 3 of the main text uses experimentally realistic parameters, Fig. S1 assumes larger  $g^2 r_b/c\Delta$  and smaller decay rates to verify that our analytical theory describes the Coulomb states accurately. Indeed, in Fig. S2, which uses the parameters of Fig. S1, we see excellent agreement between the numerical simulations and the predicted group velocity. For each  $n$ , the extracted

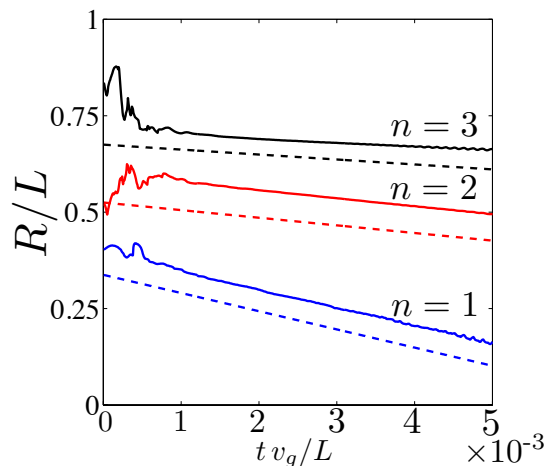


Figure S2: Time evolution of the average center of mass position of the Coulomb wave packets with parameters as in Fig. S1. The initial state is given by Eq. (S24). The horizontal axis is propagation time in units of  $L/v_g$ , while the vertical axis is defined as the average over  $r < r_b$  of the position of the peak values of the  $EE$ -component of the wavefunction, where, at each  $r$ , the peak value is defined with respect to  $R$ . The  $n = 2$  and  $3$  curves are shifted vertically for visibility. The dashed lines are the prediction for the group velocity from Eq. (5) in the main text and are also plotted with a shift relative to solid curves for visibility. The extracted slope from the linear region of the simulations agrees with the predicted group velocity to within a few percent for each  $n$ .

slope in the linear region agrees with the predicted value to within a few percent. For  $n = 1, 2$  and  $3$ , the group velocity of the Coulomb states for these parameters is approximately  $-50 \cdot v_g$ ,  $-20 \cdot v_g$  and  $-10 \cdot v_g$ , respectively.

## VI. NON-NEGATIVITY OF GROUP VELOCITY

In this section, we show that the group velocity in a system with, possibly interacting, right-going modes cannot be negative for normalizable eigenstates. Let us write the Schrödinger equation as

$$H_K |\Psi_K\rangle = \omega_K |\Psi_K\rangle, \quad (\text{S25})$$

where we have made explicit the dependence on some parameter  $K$ , which will be identified later as the total momentum of two particles. One can then see that

$$\begin{aligned} \partial_K \omega_K &= \langle \Psi_K | \partial_K H_K | \Psi_K \rangle + \omega_K \partial_K \langle \Psi_K | \Psi_K \rangle \\ &= \langle \Psi_K | \partial_K H_K | \Psi_K \rangle, \end{aligned} \quad (\text{S26})$$

where the second term in the first line vanishes for a normalized state  $\langle \Psi_K | \Psi_K \rangle = 1$ . This result is known as the Hellmann-Feynman theorem.

For our system, we can cast the Hamiltonian in the two-particle sector in the basis defined by  $(EE \ ES_+ \ ES_- \ SS)^T$ . (The generalization to the case where  $|e\rangle$  is not adiabatically eliminated is straightforward.) Identifying  $K$  with the total momentum, from Eqs. (S1-S4), we have

$$\partial_K H_K = \delta(r - r') \begin{pmatrix} c & 0 & 0 & 0 \\ 0 & c/2 & 0 & 0 \\ 0 & 0 & 0 & 0 \\ 0 & 0 & 0 & 0 \end{pmatrix}, \quad (\text{S27})$$

which is a nonnegative matrix acting on the Hilbert space associated with the relative coordinate  $r$  (the center-of-mass plane wave, although not normalizable, does not enter the argument). Therefore, the group velocity  $v_g = \partial \omega_K / \partial K$  given by Eq. (S26) cannot be negative for any eigenstate whose relative-coordinate wavefunction is normalizable.

---

\* These two authors contributed equally.

- [S1] A. V. Gorshkov, J. Otterbach, M. Fleischhauer, T. Pohl, and M. D. Lukin, Phys. Rev. Lett. **107**, 133602 (2011).
- [S2] T. Peyronel, O. Firstenberg, Q.-Y. Liang, S. Hofferberth, A. V. Gorshkov, T. Pohl, M. D. Lukin, and V. Vuletic, Nature (London) **488**, 57 (2012).
- [S3] O. Firstenberg, T. Peyronel, Q.-Y. Liang, A. V. Gorshkov, M. D. Lukin, and V. Vuletic, Nature (London) **502**, 71 (2013).
- [S4] P. Bienias, S. Choi, O. Firstenberg, M. F. Maghrebi, M. Gullans, M. D. Lukin, A. V. Gorshkov, and H. P. Büchler, Phys. Rev. A **90**, 053804 (2014).